arXiv:0908.0962v1 [astro-ph.SR] 6 Aug 2009

Time-Distance Solar Far-Side Imaging Using Three-Skip Acoustic Signals

S. Ilonidis[1] · **J. Zhao**[1] · **T. Hartlep**[2,3]

Abstract The purpose of this work is to image solar far-side active regions using acoustic signals with three skips and improve the quality of existing images. The mapping of far-side active regions was first made possible using the helioseismic holography technique by use of four-skip acoustic signals. The quality of far-side images was later improved with the combination of four- and five-skip signals using the time-distance helioseismology technique. In this work, we explore the possibility of making three-skip far-side images of active regions, and improving the image quality by combining the three-skip images with the images obtained from existing techniques. A new method of combining images is proposed that increases the signal-to-noise ratio and reduces the appearance of spurious features.

Keywords: Far-side imaging, Helioseismology, Active regions

1. Introduction

The detection of large solar active regions on the far side of the Sun can greatly improve space-weather forecasting and facilitate the study of evolution of those active regions. Active regions that appear on the east solar limb can affect space weather, causing problems in spacecraft, electrical power grids, and telecommunications. Monitoring the solar far-side activity allows for the anticipation of large active regions by more than a week before they rotate into our view from the Sun's east limb.

The first attempt to map the central region of the solar far side was made by Lindsey and Braun (2000a) by use of the helioseismic holography technique (Lindsey and Braun, 2000b). Low- and medium-ℓ acoustic waves exhibit an

[1] W. W. Hansen Experimental Physics Laboratory, Stanford
University, Stanford, CA 94305-4085, USA
email: ilonidis@sun.stanford.edu
[2] NASA Ames Research Center, MS 230-2, Moffett Field,
CA 94035-1000, USA
[3] present address: W. W. Hansen Experimental Physics
Laboratory, Stanford University, Stanford, CA 94305-4085,
USA

apparent travel time deficit in solar active regions which is detectable by phase-sensitive holography (Braun and Lindsey, 2000). This technique initially included only double-skip acoustic signals but was later extended (Braun and Lindsey, 2001) to map the whole far side using single- and triple-skip signals.

The time-distance helioseismology technique also has the capability to map the central area of the solar far side (Duvall, Kosovichev, and Scherrer, 2000; Duvall and Kosovichev, 2001). The mapping area was later extended onto the whole far side using four- and five-skip acoustic signals (Zhao, 2007). The two schemes are used separately to make two whole far-side maps. The combination of the two maps gives far-side images with better signal-to-noise ratio. This is an independent solar far-side imaging tool in addition to the holography technique which allows for the possibility to cross-check the active regions seen in both time-distance and helioseismic holography techniques and hence improves the accuracy of monitoring the solar far-side active regions.

However, no studies have been carried out yet to explore the possibility of making far-side images using acoustic signals with three skips. In this paper we apply the time-distance technique to show that it is possible to image the solar far side utilizing three-skip acoustic signals, and discuss advantages and disadvantages of this method. We also suggest a method to improve the quality of existing far-side images that includes the results of our work.

2. Data and Technique

The medium-ℓ program of the *Solar and Heliospheric Observatory* / Michelson Doppler Imager (SOHO/MDI) (Scherrer *et al.*, 1995) is used in this work. The oscillation modes that are observed range from $\ell = 0$ to ≈ 300 and the data are acquired with one-minute cadence and a spatial sampling of $10''$ (0.6 heliographic degrees per pixel). The $\ell - \nu$ power spectrum diagram of this dataset is shown in Figure 1a. The continuity of the observations and the particular range of modes that we analyze make the medium-ℓ data ideal for solar far-side imaging.

The time-distance technique is able to detect acoustic signals that travel to the far side and return to the front side after experiencing four and five skips (Zhao 2007). It is useful to examine whether acoustic signals after three skips are also detectable by this technique. In Figure 1b the time-distance diagram is computed using all oscillation modes from a 2048-minute MDI medium-ℓ dataset with a spatial size of $120° \times 120°$ after the region is tracked with the Carrington rotation rate and is remapped using Postel's projection with the solar disk center as the remapping center. The diagram shows acoustic skips of up to seven times on the front side as well as signals traveling to the far side and returning to the front side after three and four skips. From all of these signals we keep only the ones that are needed in our analysis and filter out all other acoustic modes. The acoustic signals that are needed should have long single-skip travel distance corresponding to low-ℓ modes. Such a filtering improves the signal-to-noise ratio at the required travel distances of the three-skip method. Figure 1c shows the time-distance diagram computed using only the useful acoustic modes with a box of ℓ-range $6-15$ at 2.5 mHz and $12-30$ at 4.5 mHz. This filtering is applied to the
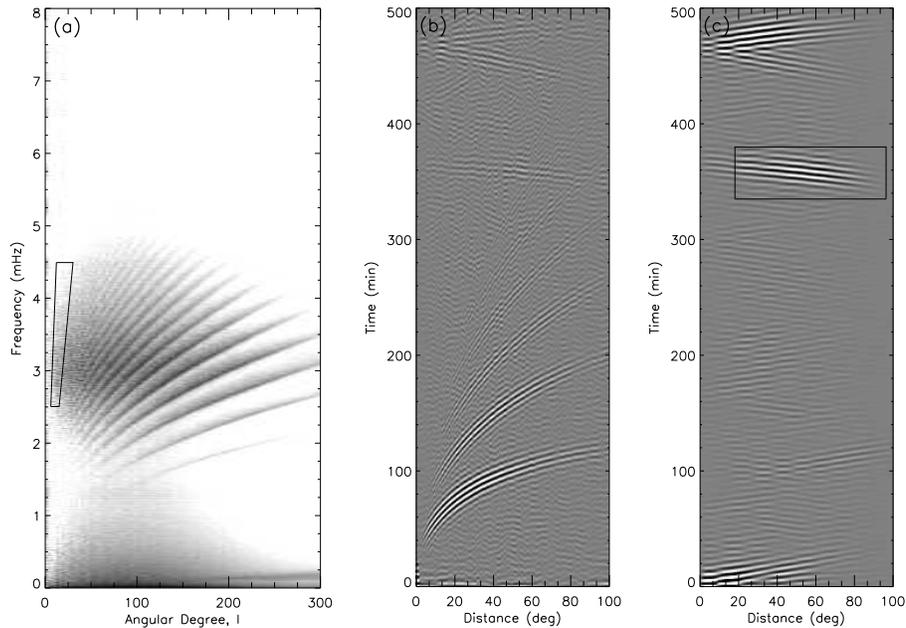
Figure 1. (a) Power spectrum computed from a 2048-minute MDI medium-ℓ dataset, (b) time-distance diagram computed using the whole power spectrum of the same dataset, and (c) time-distance diagram computed using only the oscillations that have frequency and ℓ included in the black quadrangle as indicated in (a). The black box delimits the acoustic travel distances and times used for far-side imaging.

data after Postel's projection and thus it works best where the geometry is least distorted. Another issue is that the theoretical travel time is a few minutes off from the time-distance group travel time after three skips, because as pointed out by Kosovichev and Duvall (1996) and Duvall *et al.* (1997), the ray-approximated travel time is a few minutes off from the time-distance group travel time.

Not all acoustic signals that come back from the far side after three skips are used but only those with time-distance annulus radii $80° − 113°$ from the target point for the single-skip and $160° − 226°$ for the double-skip (see Figure 2). This scheme is able to cover the whole far side except for a circular region in the center of that side. Following Zhao (2007) to save computation time, only the areas lower than the latitude of $48°$, where nearly all active regions are located, are included in the far-side imaging computations.

The first step of the computational procedure is to track a 2048-minute long MDI medium-ℓ dataset with the Carrington rotation rate. Then it is remapped to Postel's coordinates centered on the solar disk with a spatial sampling of $0.6°$ per pixel, covering a span of $120°$ along the Equator and the central meridian. This dataset is filtered in the Fourier domain and only the oscillation modes with travel distances in agreement with the distances listed above are kept. Corresponding pixels in the annuli on both sides of the target point are selected and the cross-covariances with both positive and negative travel time lags are
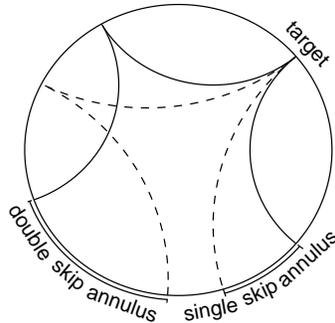
Figure 2. Sketch for the three-skip measurement scheme where one set of single-skip and one set of double-skip rays are located on the either side of the target point.

computed. Then both time lags are combined and all cross-covariances obtained from different distances after appropriate shifts in time are also combined. The final cross-covariance is fitted with a Gabor wavelet function (Kosovichev and Duvall, 1996) and an acoustic phase travel time is obtained. The far-side image is a display of the measured mean acoustic travel times after a Gaussian smoothing with a FWHM of 2.0°.

3. Results

3.1. Results from Numerical Simulation Data

It is still not clear how accurate the far-side imaging techniques are. Comparing the far-side images with the directly observed near side after active regions have rotated into our view from the far side, or before they rotate out of view onto the far side, is the traditional way to evaluate the accuracy of far-side images. However, active regions sometimes develop rapidly, on time scales of days, thus the traditional way is not always sufficient. Numerical models of solar oscillations can provide artificial data with near-surface perturbations mimicking active regions on the far side of the Sun. Applying helioseismic imaging techniques on the simulated wavefield allows for a direct comparison of the far-side images with the prescribed sound speed perturbations, and it thus provides a more accurate test of the far-side imaging technique.

We present results on testing the new time-distance technique with three-skip acoustic signals. The sensitivity of the technique is tested by varying the size of the active region. The propagation of solar acoustic waves is simulated numerically in a spherical domain. The simulations take into account the effects
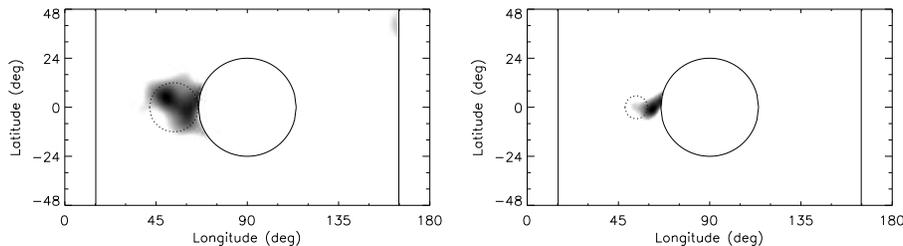
Figure 3. Far-side images for simulations with an active region with radius 180 Mm (left) and 90 Mm (right). The dotted circles indicate the sizes and locations of active regions.

of a spatially varying sound speed but for now ignore flows or magnetic fields. The quiet solar medium is represented with having a sound speed that is only a function of radius given by the standard solar model S of Christensen-Dalsgaard *et al.* (1996) matched to a chromospheric model from Vernazza, Avrett, and Loeser (1981). Active regions are modeled as local variations in the sound speed from the quiet Sun. The depth profile of these variations can be found in Hartlep *et al.* (2008). The data are prepared to be similar to MDI medium-ℓ data and have been used to test the existing four- and five-skip far-side imaging technique (Hartlep *et al.*, 2008). The radial velocity is computed at a location 300 km above the photosphere and is stored with one-minute cadence and a spatial resolution of $0.703°$ pixel^{-1}. The data are remapped onto Postel's coordinates with a spatial sampling of $0.6°$ pixel^{-1}. A region of $120° \times 120°$ is used for analysis and the first 500 minutes are discarded because they represent transient behavior. The following 1024 minutes are used in the analysis, a short but sufficient period for far-side analysis. The rest of the procedure for the simulation data is the same as for the observations. For more details about the simulation and for discussion on how these simulations were used for testing far-side imaging, see Hartlep *et al.* (2008).

We have used simulated data for two active-region sizes, a large one with a radius of 180 Mm and a smaller one with a radius of 90 Mm. A circular area around the center of the far side with a radius of $24°$ as well as a band along the solar limb $15°$ in width have been excluded from the far-side map because the three-skip technique is not able to fully cover these areas. As seen in the left image of Figure 3, the three-skip scheme can clearly detect the large active region but with some level of uncertainty in the location as well as the shape of the region. The detection of the small active region by the three-skip scheme is shown in the right image of Figure 3. It is quite remarkable that the far-side map is completely clear of spurious features. However, as in the previous case, the location and the shape are slightly different from the original region.

3.2. Results from MDI observations

We have applied our three-skip imaging technique to the numerical simulation data and found that this technique is able to recover active regions larger than at least 90 Mm in size, but unable to detect unambiguously features close to the far-side limbs and center due to the low, or no, acoustic wave coverage in these areas.

Next we make far-side images using MDI observational data. Two different datasets, each lasting 2048 minutes, with the middle time corresponding to 12:00 UT of 8 and 9 November 2003, are used for this purpose, and the corresponding maps are shown on the left side of Figures 4 and 5 respectively. In order to highlight the far-side active regions, the same maps are shown on the right side of Figures 4 and 5 after applying a travel time threshold of $-2.0\ \sigma$. The threshold for the three-skip image is smaller ($-1.5\ \sigma$) because the standard deviation of this travel time map is substantially larger than other maps averaged from two or three travel time maps. In the first row of Figures 4 and 5, far-side images made with the new three-skip technique are displayed. In order to test the quality and accuracy of the new imaging technique, far-side images from the same dates made with the existing time-distance technique (Zhao, 2007) are shown in the second row. The third and fourth rows display far-side images made with a combination of three-, four-, and five-skip results, but the technique applied for the combination is different in each case, and it is further discussed in more details below.

The new far-side maps that utilize acoustic signals with three, four, and five skips consist of three distinct regions, two bands along the solar limbs 15° in width, a circular area around the center of the far side with a radius of 24°, and the rest of the far-side region. The imaging of the bands along the solar limbs is based only on acoustic signals with four skips. A combination of four- and five-skip acoustic signals is used for the central circular area, while for the rest of the far-side image the combination includes three-skip measurements in addition to the four- and five-skip measurements. The imaging of the existing far-side maps is based on a combination of four- and five-skip measurements except for two bands along the solar limbs where only four-skip measurements are used (see Zhao, 2007). The boundaries of all of those regions have been linearly smoothed over a distance of 12°. All of the far-side acoustic travel times are displayed after a mean travel time background is removed.

As mentioned before, the two bottom rows of Figures 4 and 5 present far-side images made by combining three-, four- and five-skip measurement schemes. The method of combining images by simply taking the average is a rather simple but reasonable technique in the case of two images and is able to enhance the signal-to-noise ratio in the far-side images (Zhao, 2007). Therefore, the arithmetic average is used in the central circular area of the far side that involves only acoustic signals with four and five skips. However, more sophisticated techniques of combination can be applied if three or more far-side images are available. At each pixel location of the far-side map where there is overlap between the regions accessed by the different combinations of skip distances, the travel times obtained from the three-, four-, and five-skip images are considered and the
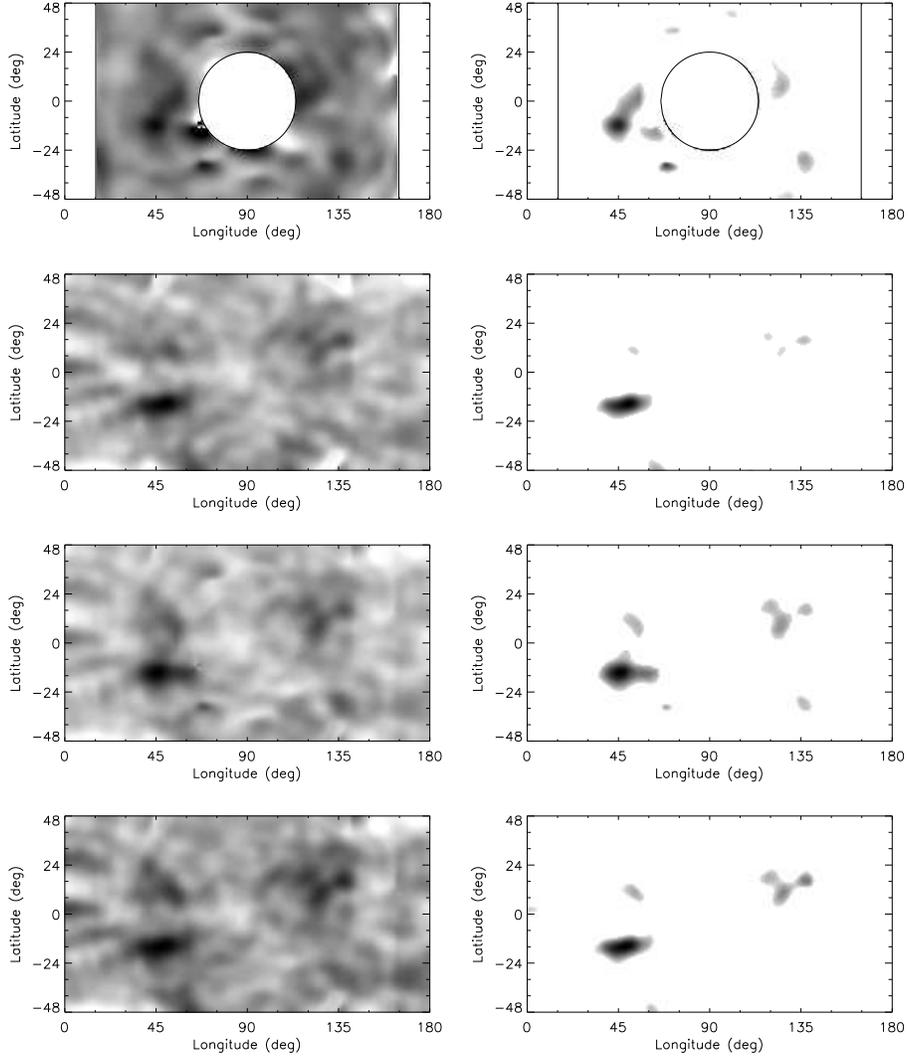
Figure 4. Results of time-distance far-side active region imaging, obtained from three-skip measurements (first row), combination of four- and five-skip measurements (second row), combination of three-, four-, and five-skip measurements by simple averaging (third row) and combination of three-, four-, and five-skip measurements by the new method of averaging (bottom row). On the right-side, images display the far-side map after applying a travel-time threshold of $-2.0\,\sigma$ ($-1.5\,\sigma$ for the three-skip map because the standard deviation is substantially larger) in order to highlight the far-side active regions that are of our interest. Images are obtained for 8 November 2003.
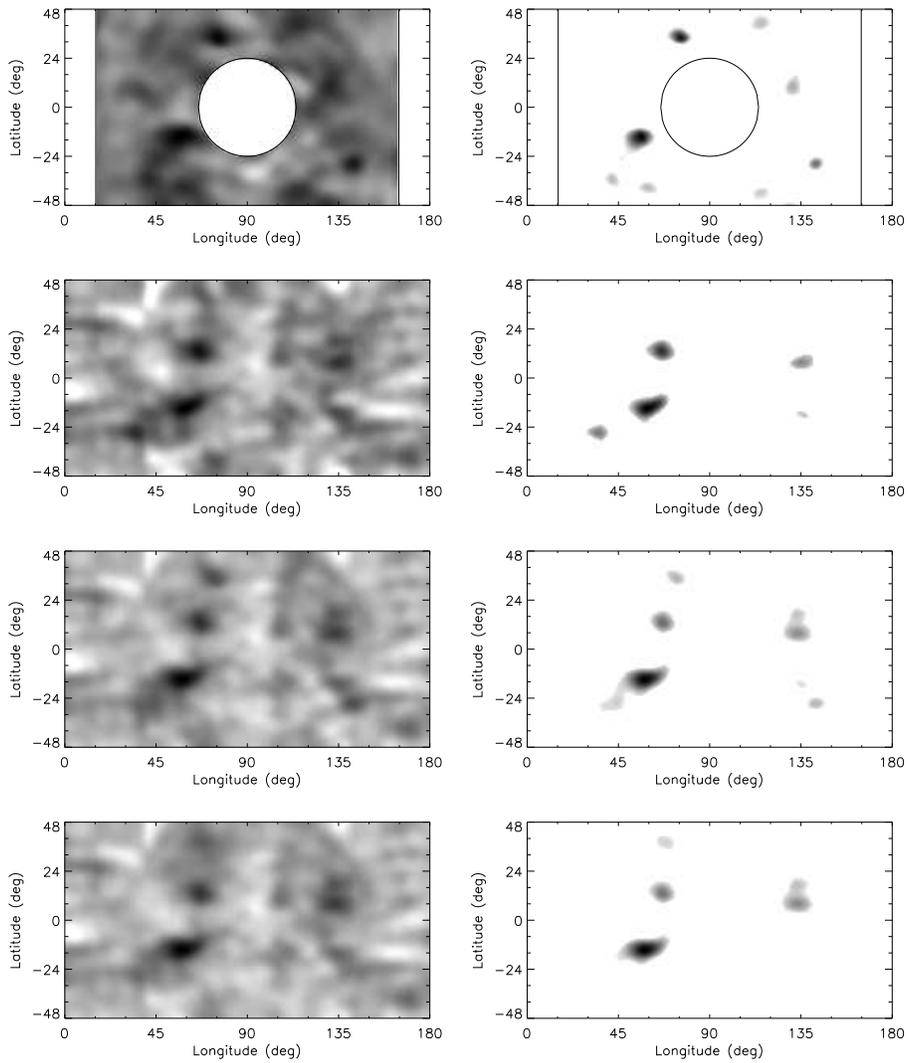
Figure 5. Same as Figure 4, but results for 9 November, 2003.

absolute values of the three differences in the travel times are calculated. If the two largest differences are larger than a high threshold and the smallest difference is smaller than a low threshold then the travel time that is substantially smaller or larger is replaced by the average of the other two. The travel time at those pixels that satisfy the above conditions is essentially the average of travel times of just two different measurement schemes. By setting the high threshold equal to 13 seconds and the low threshold equal to 9 seconds we have managed to

remove spurious features from the far-side map and at the same time enhance the signal in the active regions. The third and fourth rows of Figures 4 and 5 show respectively far-side maps made by simply averaging the three-, four-, and five-skip acoustic signals and by applying the new combination technique.

Both the new and the existing far-side imaging technique cannot give consistently a clear far-side map without any spurious features but they can differ quantitatively as well as qualitatively. It is clear from Figure 4 and 5 that the level of noise in the three-skip image is quite high. If we simply average the three-, four-, and five-skip signals and compare the new far-side map with the existing map, the large active regions appear larger and more enhanced but spurious signals originating from the contribution of the noisy three-skip image also appear in the far-side map. However, the new combination technique is able either to completely remove some of those signals from the far-side map or at least to weaken their contribution. As a result the new far-side maps have a better signal-to-noise ratio with reduced and fewer artifacts.

Comparing corresponding maps we can conclude that the detection of large active regions is more successful with the new technique. The three-skip measurement scheme utilizes low-ℓ acoustic modes, lower than the ones used in the four- and five-skip schemes hence the wavelength of these modes is greater, and this results in a reduced sensitivity in the detection of small active regions. But even if the three-skip scheme completely failed to detect small active regions, the new combination technique ensures that in most cases these regions will be visible in the far-side map. On the other hand, increasing the total number of skips produces degradation in the signal correlations and, as we expect, the three-skip method has stronger correlations than the four- and the five-skip method. It is quite remarkable though that in some cases the three measurement schemes have spurious signals at the same locations, an indication that there might be some weak correlation in the noise of the far-side images, or alternatively, that "ghost-images" from near-side active regions appear on the far side.

4. Discussion

The availability of both time-distance and helioseismic holography far-side maps makes the detection of active regions more robust and confident. Additionally, far-side imaging provides us with some experience in analyzing low- and medium-ℓ mode oscillations by the use of local-helioseismology techniques and this will help us in analyzing deeper solar interior and polar areas.

The time-distance technique with three-skip acoustic signals is another imaging tool in addition to the existing techniques. We have successfully made three-skip far-side images of the solar active regions using data from numerical simulations as well as from MDI observations. The three-skip measurement scheme cannot cover the whole far side, and moreover, the far-side images have many spurious features that do not appear in the four- and five-skip images. Consequently the three-skip images by themselves are not as good as the images obtained by other time-distance techniques. Our motivation for making three-skip far-side images derives from the fact that the availability of one more

far-side imaging technique makes possible the application of more sophisticated methods of combining images than the simple arithmetic averaging. In addition, the correlations in the three-skip technique are rather strong and facilitate the detection of large active regions.

The combination of four- and five-skip measurement schemes was shown by Zhao (2007) to significantly enhance the signal-to-noise ratio of far-side acoustic travel time measurements and make the resulting far-side map much cleaner. More specifically it helps to remove most but not all of the spurious features. On the other hand it also removes some small active regions that can otherwise be seen in one map or the other. The three-skip scheme is an independent tool for imaging the far-side solar active regions and thus it can be combined with the two existing time-distance techniques. The combination of the three measurements can give a cleaner far-side map, with fewer spurious features and enhanced active regions.

The method of combining images is very important in the problem of far-side imaging. In this paper we present two different methods, the first one was also used by Zhao (2007) while the second one is a newly suggested method that improves the quality of the image. The new method utilizes, at each pixel location, the far-side maps derived from three-, four-, and five-skip travel times, subject to two arbitrary thresholds. Properly adjusting these thresholds it is possible to enhance the active regions and reduce the level of noise.

References

Braun, D.C., Lindsey, C.: 2000, *Solar Phys.* **192**, 307.

Braun, D.C., Lindsey, C.: 2001, *Astrophys. J.* **560**, L189.

Christensen-Dalsgaard, J., Däppen W., Ajukov, S.V., Anderson, E.R., Antia, H.M., Basu, S., Baturin, V.A., Berthomieu, G., Chaboyer, B., Chitre, S.M., *et al.*: 1996, *Science*, **272**, 1286.

Duvall, T.L. Jr., Kosovichev, A.G.: 2001, In: Brekke, P., Fleck, B., Gurman, J.B. (eds.) *IAU Symp. 203, Recent Insights into the Physics of the Sun and Heliosphere: Highlights from SOHO and Other Space Missions*, Astron. Soc. Pac., San Francisco, 159.

Duvall, T.L. Jr., Kosovichev, A.G., Scherrer, P.H.: 2000, *BAAS*, **32**, 837.

Duvall, T.L. Jr., Kosovichev, A.G., Scherrer, P.H., Bogart, R.S., Bush, R.I., De Forest, C., Hoeksema, J.T., Schou, J., Saba, J.L.R., Tarbell, T.D., *et al* 1997, *Solar Phys.*, **170**, 63.

Hartlep, T., Zhao, J., Mansour, N.N., Kosovichev, A.G.: 2008, *Astrophys. J.* **689**, 1373.

Kosovichev, A.G., Duvall, T.L. Jr.: 1996, In: Pijpers, F.P., Christensen-Dalsgaard, J., Rosenthal, C.S. (eds.) *Proc. SCORe'96 Workshop: Solar Convection and Oscillations and Their Relationship*, (Dordrecht: Kluwer), 241.

Lindsey, C., Braun, D.C.: 2000a, *Science* **287**, 1799.

Lindsey, C., Braun, D.C.: 2000b, *Solar Phys.* **192**, 261.

Scherrer, P.H., Bogart, R.S.,Bush, R.I., Hoeksema, J.T., Kosovichev, A.G., Schou, J., Rosenberg, W., Springer, L., Tarbell, T.D., Title, A., *et al.*: 1995, *Solar Phys.* **162**, 129.

Vernazza, J.E., Avrett, E.H., Loeser, R.: 1981, *Astrophys. J. Suppl.* **45**, 635.

Zhao, J.: 2007, *Astrophys. J.* **664**, L139.